Hindawi
Geofluids
Volume 2022, Article ID 8063469, 11 pages
https://doi.org/10.1155/2022/8063469

Research Article

Predicting Time-to-Failure of Red Sandstone by Temporal Precursor of Acoustic Emission Signals

Ansen Gao[1], **Chengzhi Qi**[1,2,3], **Renliang Shan**[1] and **Chunlai Wang**[4]

[1]*School of Mechanics and Civil Engineering, China University of Mining and Technology (Beijing), Beijing 100083, China*
[2]*School of Civil and Transportation Engineering, Beijing University of Civil Engineering and Architecture, Beijing 100044, China*
[3]*Beijing Advanced Innovation Centre for Future Urban Design, Beijing University of Civil Engineering and Architecture, Beijing 100044, China*
[4]*School of Energy and Mining Engineering, China University of Mining and Technology (Beijing), Beijing 100083, China*

Correspondence should be addressed to Ansen Gao; gaoansen@163.com and Chengzhi Qi; buceaqcz@163.com

Received 18 March 2022; Accepted 8 June 2022; Published 18 July 2022

Academic Editor: Zhijie Wen

The evolution pattern of rock damage is a progressive failure process of rock materials. It is the basis for predicting failure time of rock materials. By theoretical and experimental analysis, the acoustic emission (AE) precursor characteristics of rock fracture and the gradual evolution pattern of rock damage were analyzed detailedly. Then, the time-to-failure of red sandstone was predicted and compared by several different methods. The results demonstrated that the failure process of red sandstone can be divided into the stable deformation stage and the critical acceleration failure stage. In the critical acceleration failure stage, the AE precursor of rock failure was easy to be observed, and the AE event rate occurred as jump-like increase phenomenon. Moreover, the gradual evolution pattern of rock damage obeyed an exponential function, and the damage acceleration phenomenon existed in the critical failure stage. Furthermore, the higher values of the average of rock damage was, the more obvious linear evolution pattern will be, which was beneficial to improve the prediction accuracy of time-to-failure of rocks. Clearly, the linear prediction results of rock failure time, after taking average values of five rock damage variables, had more higher accuracy when damage variable exceeded $D = 0.5$. The predicting result of specimen R1 was 0.2 s ahead of its actual failure time, and the predicting result of specimen R6 was 8.1 s ahead of its actual failure time. Therefore, this method is meaningful and it can be used for the early warning of rockburst.

1. Introduction

The crack initiation to rock fracture is accompanied by acoustic emission (AE) phenomenon. It is very useful for revealing the failure mechanism of rock materials [1], and it is particularly effective for monitoring the physics precursor of natural events such as earthquake and rockburst. Typically, the accelerating phenomenon of AE monitoring signals is observed before the failure of rock materials [2–5]. It means that there is a critical failure stage of rocks, and it is very important to make full use of the critical AE precursor to elucidate the failure mechanism of rock materials. Therefore, it is an important challenge to present a quantitative method for forecasting time-to-failure of rocks.

Rockburst always occurs in the excavation process of tunneling and mining, which seriously endangers the safety of engineering structures [6, 7]. In many cases, the precursor of seismic activity showed acceleration phenomenon which can be used as a robust precursor of volcanic eruptions [8]. Meanwhile, many rockbursts were preceded by increases of AE monitoring signals [2–5, 9]. A range of different models have been proposed to relate the evolution of AE monitoring signals to the onset time of rockburst. Fukuzuno [10] used an empirical power law to model the evolution of surface displacements prior to slope failure. Later on, Voight [8] proposed a general material failure law to characterize the evolution pattern of rock deformation and AE signals. Nevertheless, Voight's model required that the failure pattern of

materials must conform to a power-law relationship, which was not friendly to the non-power-law evolution pattern of rock failure. Boué et al. [11] presented an approach for real-time monitoring volcano-seismic precursors. It can forecast the eruption time before it erupting. However, the time scale of this method was relatively large and inaccurate, and the accuracy of predicting time-to-failure of rock materials was still unclearly.

Rock fracture is driven by the stress and the time-dependent cracking process [12]. The time-dependent fracture behavior is particularly important for rock engineering structures for long-term stability [13]. However, the turning point of the stable and unstable deformation stage of rocks has not been quantitatively distinguished [13]. The time series of daily seismic event rate for Kilauea Volcano from 1959 to 2000 was analyzed by Chastin et al. [14]. It showed that an accelerating behavior of the mean seismic event rate emerged 10-15 days before the eruption. Still, the predicting time scale was measured in days, and it was relatively large and fuzzy [14]. The determined accelerating behavior of average seismic events seems to give us some insights for the time-to-failure of sudden disasters such as volcanic eruption and rockburst. The onset time of acceleration phenomenon is the better evaluation indicator for materials failure prediction [15]. Despite the widespread interest in predicting failure time of rocks, the starting point of damage acceleration was not reliably identified. This usually resulted in a lag in predicting time-to-failure of rock materials. It can decrease the possibility of false alarms of rockburst by accurately identifying the starting point of rock damage acceleration stage [2–5, 9]. Therefore, a credible method is still required to identify the starting point of damage acceleration process for predicting time-to-failure of rocks.

The AE signals monitoring technology has been verified as an effective, nondestruction, and real-time monitoring tool, which reliably reflects the nucleation and propagation of irreversible microcracks before rock failure. In this study, we focused on methods for forecasting the time-to-failure of a forthcoming rockburst based on damage accelerating phenomenon of AE signals. Firstly, the internal damage evolution model of rocks was revealed by theoretical derivation. Then, the red sandstone specimens were subjected to the uniaxial compression test. The AE precursor of rock failure and the evolution pattern of rock damage were analyzed based on AE event rate. Moreover, the time-to-failure of rocks was further predicted and compared by linear and exponential function methods.

2. Theoretical Basis

The damage acceleration behavior exists in the critical failure stage of rock materials, and it is very meaningful for better identifying the damage evolution pattern and predicting time-to-failure of rock materials [15]. Before analyzing and calculating rock damage variables, the following assumptions are made for simplification: (i) rock materials are isotropic, homogenous, continuous, and brittle materials with preexisting microcracks on a macroscale; (ii) the elastic damage constitutive law is applicable to each mesoscopic element; (iii) rock damage is continuously developed and gradual accumulation in mesoscopic elements; (iv) the strength of mesoscopic elements is observed following Weibull distribution function [16–18].

$$P(F) = \begin{cases} \dfrac{m}{F_0}\left(\dfrac{F}{F_0}\right)^{m-1} \exp\left[-\left(\dfrac{F}{F_0}\right)^{m}\right] & F > 0, \\ 0 & F \le 0, \end{cases} \tag{1}$$

where F is an elemental strength parameter or stress level, F_0 is its mean value, and m is the shape parameter (Weibull modulus) or a homogeneous index of rock materials which measures the concentration of F.

Then, let N denotes the number of all mesoscopic elements, and N_f denotes the number of all failed mesoscopic elements. The damage variable (D) can be directly defined as the following equation.

$$D = \frac{N_f}{N}. \tag{2}$$

When the stress level F increases to $F + dF$, the number of failed mesoscopic elements increases by $NP(F)dF$. If external force increases from zero to F, from equation (1), the total number of failed mesoscopic elements is calculated by the following equation.

$$N_f(F) = \int_0^F NP(y)dy = N\left\{1 - \exp\left[-\left(\frac{F}{F_0}\right)^{m}\right]\right\}. \tag{3}$$

Then, from equations (2) and (3), the following equation can be obtained.

$$D = 1 - \exp\left[-\left(\frac{F}{F_0}\right)\right]^{m}. \tag{4}$$

It is assumed that the ultimate principal stress for rock failure meets the Hoek-Brown strength criterion [19].

$$F(\sigma) = n\sigma_c \frac{I_1^*}{3} + 4J_2^* \cos^2\theta_\sigma + n\sigma_c\sqrt{J_2^*}\left(\cos\theta_\sigma + \frac{\sin\theta_\sigma}{\sqrt{3}}\right) = s\sigma_c^2, \tag{5}$$

where σ_c is the uniaxial compressive strength, n and s are the material constants, θ_σ is Lode's angle, I_1^* is the first invariant of effective stress, and J_2^* is the second invariant of effective stress deviators.

For the uniaxial compression, $\sigma_2 = \sigma_3 = 0$, $\theta_\sigma = 30^\circ$, there are the following determinate relationships.

$$I_1^* = E\varepsilon_1, \tag{6}$$

$$\sqrt{J_2^*} = \frac{E\varepsilon_1}{\sqrt{3}}, \tag{7}$$

where E is the modulus of elasticity and ε_1 is the axial strain.

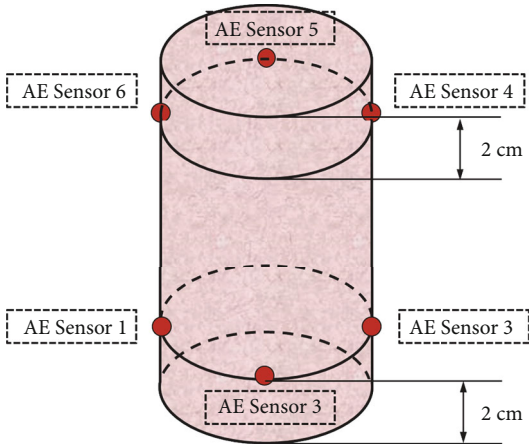

Figure 1: Schematic diagram of AE sensors distribution.

Substituting equations (6) and (7) into (5), the following equation can be obtained.

$$F(\sigma) = n\sigma_c E\varepsilon_1 + (E\varepsilon_1)^2. \tag{8}$$

According to equations (4) and (8), the mechanical damage (D) caused by the compression stress is as the following equation.

$$D = 1 - \exp\left\{-\left[\frac{n\sigma_c E\varepsilon_1}{F_0} + \frac{E^2\varepsilon_1^2}{F_0}\right]^a\right\}. \tag{9}$$

This is the damage evolution equation of mesoscopic elements in the statistical constitutive model of rock materials. Equation (9) can be simplified as the following equation.

$$D = 1 - \exp\left[-\left(\alpha\varepsilon_1 + \beta\varepsilon_1^2\right)^a\right], \tag{10}$$

where $\alpha = n\sigma_c E/F_0$ and $\beta = E^2/F_0$.

Then, assuming that rock materials have no initial damage, the cumulative number of AE events is N_{AW} when rock is completely broken. For any deformation time t, the cumulative number of AE events is $N_A(t)$. Then, the following damage equation can be defined by AE events.

$$D = \frac{N_A(t)}{N_{AW}}. \tag{11}$$

3. Experimental Investigation

3.1. Experimental Equipment. The Instron 5985 compression testing machine was used in this study, which had a maximum load capacity of 250 kN and the minimum loading rate of 0.0001 mm/min. The AE monitoring equipment employed PCI-II, which was an AE signals acquisition and analysis system. To improve the spatial positioning accuracy of AE events, six AE sensors were used in this test and they were placed 20 mm away from both ends of rock specimens, as shown in Figure 1. In addition, the AE sensors were distributed at an angle of 90° to ensure they were not coplanar.

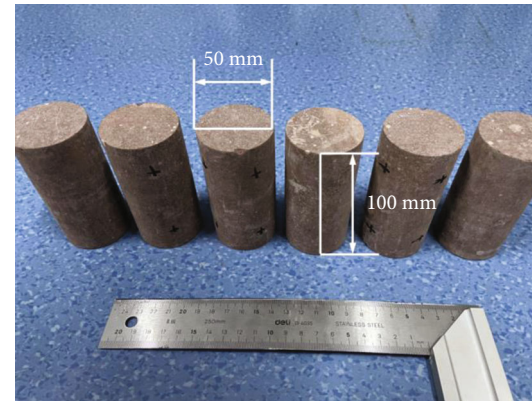

Figure 2: The prepared red sandstone specimens.

The threshold value of the AE monitoring system was set to 45 dB, the preamplifier gain was set to 40 dB, and the sampling frequency was set to 1 MHz.

3.2. Specimen Preparation. The same raw rock sample was used for preparing rock specimens to ensure the physical and mechanical parameters of specimens had the same level of magnitude. Then, the specimens were prepared as cylinder with a height-diameter ratio of 2 : 1 (with the size of 100 : 50 mm). After preliminary preparation, the specimens were carefully polished to ensure both ends were ground flat without significant damage, as shown in Figure 2.

3.3. Experimental Method. For verifying the rationality of the damage evolution model and the method of predicting time-to-failure of rocks, six red sandstone specimens were used for this study. For specimens R1~R3, their loading rate was 0.1 mm/min, and for specimens R4~R6, their loading rate was 0.03 mm/min. The loading process was monitored synchronously with AE signals monitoring process. Beyond peak stress, the loading process was stopped after the stress dropped to 80% of its peak value to ensure rock specimens had been completely destroyed. In particular, the representative results of specimens R1 and R6 were used to analyze in this study.

4. Results

4.1. The Evolution Characteristics of AE Signals of Red Sandstone. Figure 3 shows the evolution characteristics of AE events with the increasing axial loading. To illustrate, Figure 3(a) is the result of specimen R1, and Figure 3(b) is the result of specimen R6. The results showed that the failure process of red sandstone needed to experience stable elastic deformation firstly, the stress increased steadily, and the stress curve was smooth. Subsequently, rock specimens entered the critical fracture stage, the stress was fluctuating and unstable, and the peak stress will be reached in a short time. Then, the stress decreased slightly in steps which was followed by the complete penetration of cracks. During the elastic deformation stage (Stage I), the AE events had relatively lower values and fewer numbers, and its variation was relatively stable and smooth. In the critical acceleration

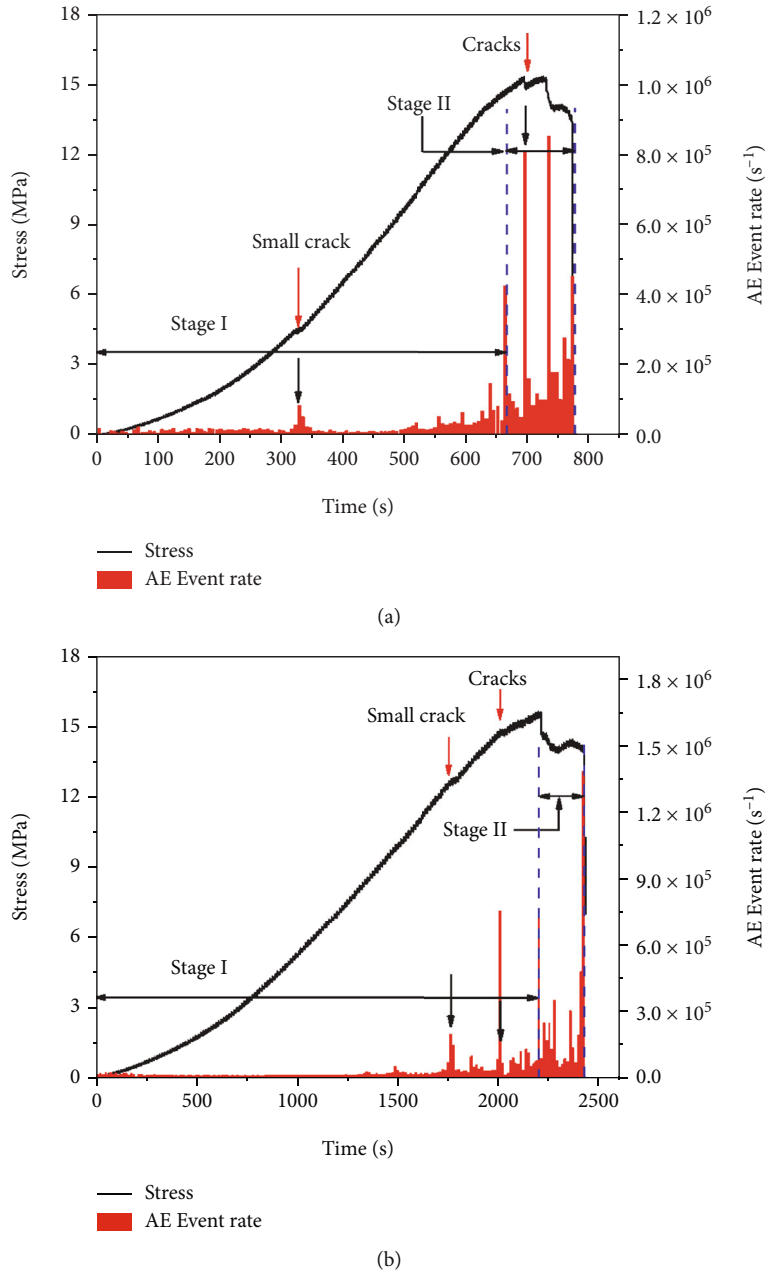

Figure 3: The evolution characteristics of AE signals. (a) The result of specimen R1. (b) The result of specimen R6.

failure stage (Stage II), the evolution characteristics of AE events were obviously different from the previous stage. The jumping spurt of AE events occurred with each large fracture (crack) inside rocks. Due to the frequent occurrence of rock fractures, the AE events increased with multiple jumps. Moreover, AE events had relatively larger values, larger numbers, and more frequent fluctuation. Due to different characteristics of AE events in Stage I and Stage II, Stage I was defined as the stable deformation stage, and Stage II was defined as the accelerated failure stage. In addition, an obvious acceleration phenomenon for cumulative AE events, generated from microcrack propagation, was clearly observed nearby the failure point. The typical evolution pattern of AE events can be used as a precursor for rock failure.

Figure 4 shows the localization of AE events inside rocks in the critical failure stage, and Figure 4(a) is the result of specimen R1 when $D = 0.5$, Figure 4(b) is the result of specimen R6 when $D = 0.5$, Figure 4(c) is the result of specimen R1 when $D = 1$, and Figure 4(d) is the result of specimen R6 when $D = 1$. Moreover, the corresponding failure time is 655 s for specimen R1 in Figure 4(a), and the corresponding failure time is 2018 s for specimen R6 in Figure 4(b). It can be seen that before the critical acceleration failure stage, the high-energy AE events inside rocks were relatively few and scattered. It demonstrated that the main cracks inside

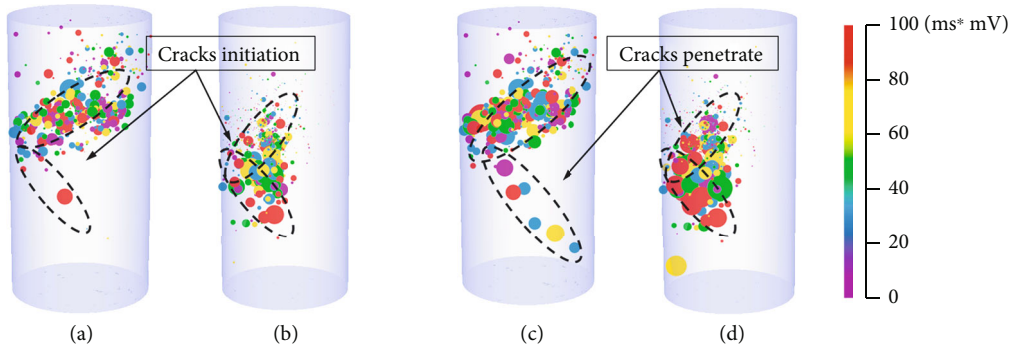

Figure 4: The fracture characteristic of red sandstone by AE events. (a) The result of specimen R1 when $D = 0.5$. (b) The result of specimen R6 when $D = 0.5$. (c) The result of specimen R1 when $D = 1$. (d) The result of specimen R6 when $D = 1$.

rock specimens had not penetrated. When rocks were completely destroyed, the distribution and morphology of main fractures (cracks) can be clearly observed. It indicated that the fracture behavior was more frequent and significant in the critical acceleration failure stage.

4.2. Identification of the Damage Acceleration Point of Red Sandstone. From equation (10), it can be seen that the damage evolution pattern of rocks is in line with the growth pattern of exponential function. Based on equation (11), the damage evolution curve of rock specimen can be calculated and plotted by AE events. Since it had been assumed that the growth pattern of rock damage obeyed the exponential law, the function $(D = y_0 + A \exp(-x/t_1))$ was used as the fitting function to analyze the damage evolution pattern of rock specimens. The fitting results indicated that this function can accurately characterize the damage evolution pattern of rocks. Furthermore, rock damage had a low-rate steady growth stage and an accelerated growth stage. From Figure 5 (Figure 5(a) is the result of specimen R1, and Figure 5(b) is the result of specimen R6), it can be known that there is a significant difference for damage growth of rock specimens before and after $D = 0.375$. Before this damage point, rock damage growth rate was relatively low and rock specimen was still in the stable deformation stage. After this damage point, rock damage growth rate began to accelerate significantly, and the damage curve became steeper. Therefore, the damage point ($D = 0.375$) can be taken as the first turning point of rock damage curve, since the turning point of stable deformation stage and the critical acceleration failure stage occurred at damage variable reaching 0.5 ($D = 0.5$). This also can be confirmed by the AE precursor in Figures 3 and 4. Therefore, for further distinguishing the evolution characteristics of rock damage, the second damage point ($D = 0.5$) can be taken as another turning point of rock damage curve. In fact, the second damage point ($D = 0.5$) was the turning point of accelerating deformation rather than the accelerating turning point of damage variables.

4.3. The Method for Predicting Time-to-Failure of Red Sandstone. As shown in Figure 5, it can be learned that rock damage has accelerated behavior in the critical failure stage. From Figure 6 (Figure 6(a) is the result of specimen R1, and Figure 6(b) is the result of specimen R6), the damage evolution characteristics, from $D = 0.375$ and $D = 0.5$ to rock failure, were further analyzed detailedly in the critical failure stage. It can be found that rock damage approximately conformed to the linear growth in the critical acceleration failure stage. Certainly, from $D = 0.375$ and $D = 0.5$ to the complete failure of rocks, the accuracy degree of linear fitting of rock damage was different. The results demonstrated that the linear evolution pattern of rock damage was more obvious and clearly when the fitting data from $D = 0.5$ to rock failure. From Figure 6, it can be seen that rock damage is not uniform, but it is grouped in several intervals. Since there are many groups of damage variables from $D = 0.375$ to rock failure, the distribution of rock damage variables was relatively discrete. Therefore, for improving the effect of linear fitting, rock damage variables were averaged from $D = 0.5$ to rock failure.

Based on the method of ordinary least squares [20], the linear fitting equation for predicting time-to-failure of rocks can be obtained. The linear fitting equation ($y = a + bx$) was used to fit the evolution curve of rock damage. For specimen R1, its actual failure time is 787.2 s ($D = 1$) in this study. For specimen R6, its actual failure time is 2432.0 s ($D = 1$) in this test. To illustrate, the negative data indicated the forecast time was advanced than the actual failure time, and the positive data indicated the forecast time was lagging behind the actual failure time. The precision of the slope for the fitting curve was only accurate to 4 digits after decimal point. Although these two fitting curves had the same slope after approximation (Figure 7(a), Line 1 and Line 2), the slopes of these two fitting curves were actually slightly different.

Table 1 compares the prediction results, by different fitting equations, with the actual failure time ($D = 1$), and it can distinguish the prediction accuracy of time-to-failure of rocks. It can be known that the fitting equations (1)~(4) (Nos. 1~4) are the results of specimen R1 and equations (5)~(8) (Nos. 5~8) are the results of specimen R6. Obviously, the fitting result of specimen R1 was better than specimen R6. The exponential growth pattern of specimen R1 was more obvious and matched, and its predicted time-to-failure of rocks was only advanced 0.7 s than the actual failure time. However, the predicted time-to-failure of specimen R6 was quite different from the actual failure time,

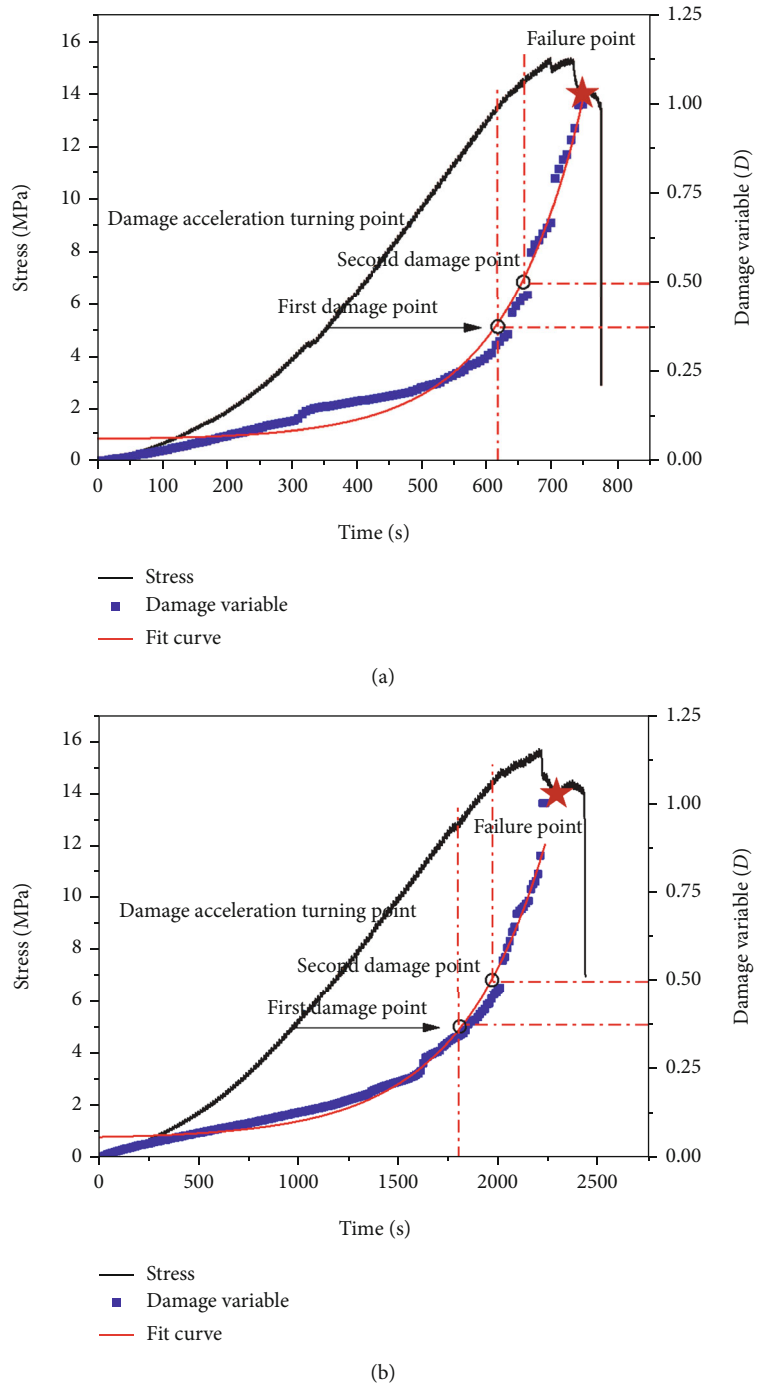

Figure 5: The damage evolution curve of red sandstone under compression. (a) The result of specimen R1. (b) The result of specimen R6.

approximately delayed 70.7 s. It demonstrated that the accuracy of predicting time-to-failure of rocks by the exponential fitting function was unstable. Then, compared with $D = 0.5$ to rock failure, the distribution of damage variables (from $D = 0.375$ to rock failure) was more scattered, and they were grouped obviously in several intervals. Then, the prediction accuracy of rock failure time was mainly analyzed from $D = 0.5$ to rock failure. Fitting equations (2) (No. 2) and (6) (No. 6) were the linear fitting equations for specimens R1 and R6 from $D = 0.5$ to rock failure, respectively. Therefore, it can be seen that the linear evolution characteristics of rock damage (from $D = 0.5$ to $D = 1$) were more obvious and clearly.

Subsequently, two different damage processing methods were used to fit damage variables, and the predicting accuracy of time-to-failure of rocks was compared. In Figure 7 (Figure 7(a) is the result of specimen R1, and Figure 7(b) is the result of specimen R6), the blue line (Line 1) was obtained by taking average of each two original damage variables. Similarly, the red line (Line 2) was obtained by taking

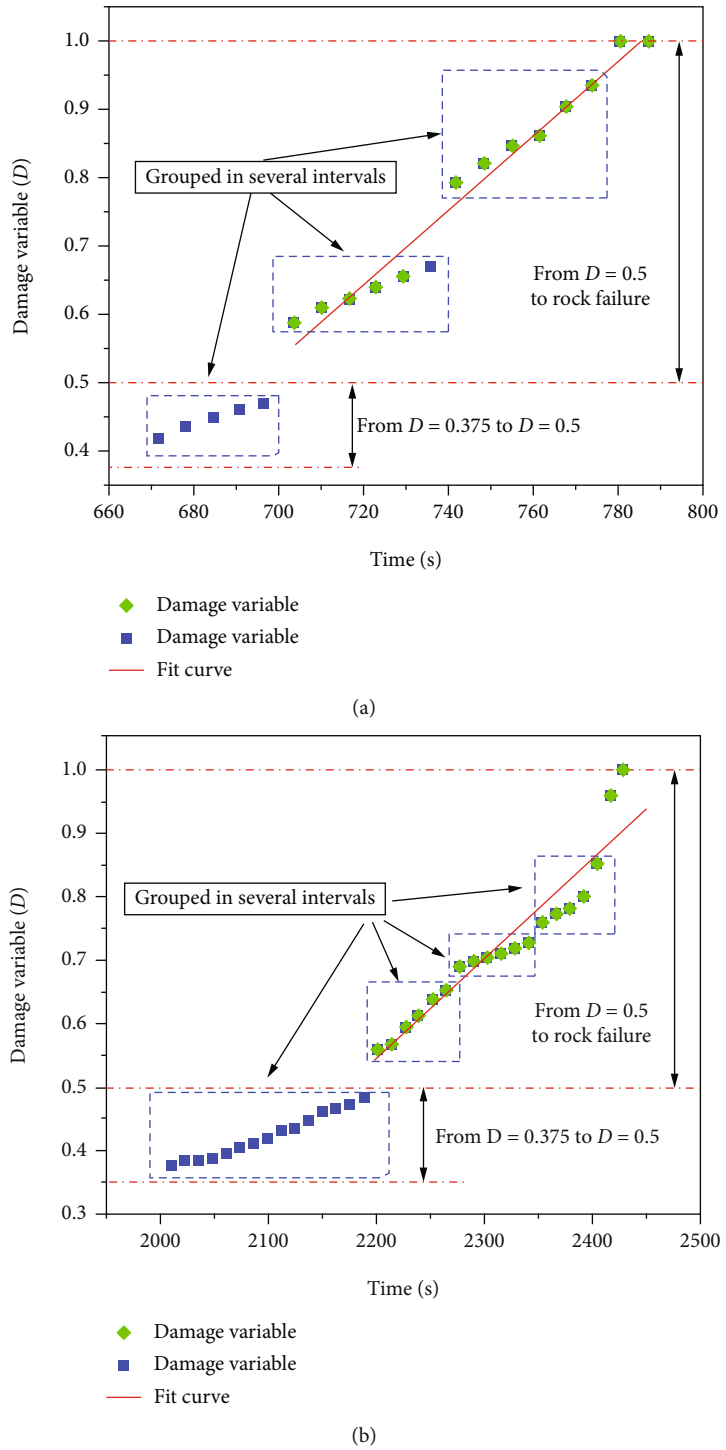

Figure 6: The damage evolution characteristic from $D = 0.375$ and $D = 0.5$ to rock failure. (a) The result of specimen R1. (b) The result of specimen R6.

average of each five original damage variables. This processing method, by taking the average values of different numbers of damage variables, can reduce the volatility of damage variables and it can improve its stationarity and accuracy of the fitting equation.

In Figure 7(a), the fitting equation for Line 1 is $y = 0.0054x - 3.24$, and its R-square is 0.9923. Likewise, the fitting equation for Line 2 is $y = 0.0053x - 3.23$, and its R-square is 0.9985. Comparing the fitting effect, it can be seen that the fitting effect of Line 2 was slightly better than Line 1. In Figure 7(b), the fitting equation for Line 1 is $y = 0.0019x - 3.90$, and its R-square is 0.9904. The fitting equation for Line 2 is $y = 0.0021x - 4.26$, and its R-square is 0.9972. For specimen R1, the fitting effect of fit equation (4) (No. 4) is

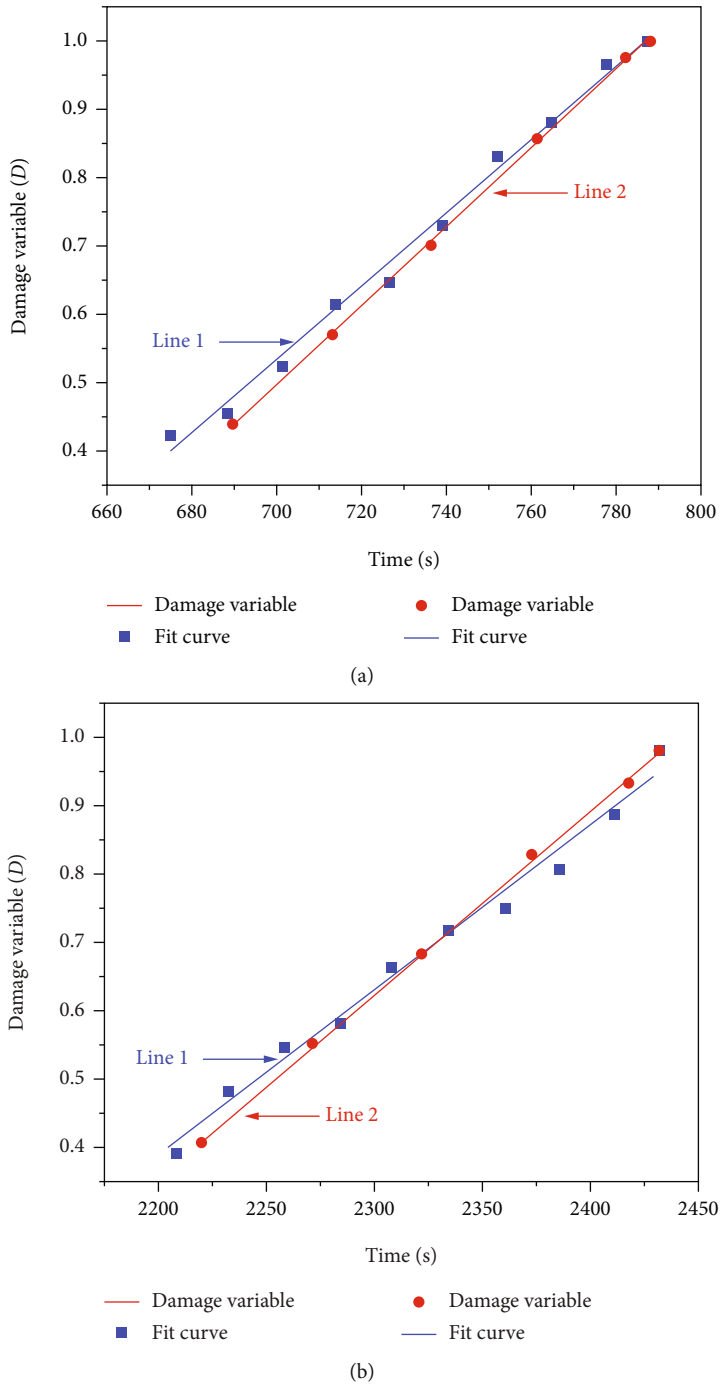

Figure 7: The damage fitting curve by different methods. (a) The result of specimen R1. (b) The result of specimen R6.

better than fit equation (3) (No. 3), and the predicted time-to-failure of specimen R1 can be advanced by 0.2 s than the actual failure time. For specimen R6, the fitting effect of fit equation (8) (No. 8) is better than fit equation (7) (No. 7), and the predicted time-to-failure of specimen R6 can be advanced by 8.1 s than the actual failure time. Hence, from $D = 0.5$ to rock failure, the predicting results of the linear function, based on the average treatment of five damage variables, were better than the predicting results of the average treatment of two damage variables. Moreover, the fitting effect of the linear function, based on averaging five damage variables, was better than the exponential function.

5. Discussions

It can be seen from Figures 3 and 4 that the evolution process of AE signals has stable deformation stage and critical acceleration failure stage. For the stable deformation stage, AE events were relatively gentle and quiet due to the overall weak damage of rocks. For the accelerated failure stage, AE

Table 1: The results of predicting time-to-failure of rocks. Nos. 1~4 are the results of specimen R1. Nos. 5~8 are the results of specimen R6.

No.	Fit data	Fit equation	R-square	Prediction time (s)	Error (s)
1	Figure 5(a)	$y = 0.063 + 0.0021 \exp(x/128.92)$	0.9725	786.5	-0.7
2	Figure 6(a)	$y = 0.0054x - 3.27$	0.9787	790.7	3.5
3	Figure 7(a), Line 1	$y = 0.0054x - 3.26$	0.9923	788.9	1.7
4	Figure 7(a), Line 2	$y = 0.0054x - 3.25$	0.9985	787.0	-0.2
5	Figure 5(b)	$y = 0.054 + 0.0049 \exp(x/475.52)$	0.9824	2502.7	70.7
6	Figure 6(b)	$y = 0.0013x - 2.25$	0.9737	2500.0	68.0
7	Figure 7(b), Line 1	$y = 0.0019x - 3.71$	0.9904	2478.9	46.9
8	Figure 7(b), Line 2	$y = 0.0021x - 4.09$	0.9972	2423.8	-8.1

events fluctuated greatly with a small fluctuation of stress, which indicated that a large number of cracks had been initiated inside specimens, and the damage increased rapidly. It had entered a critical failure stage. It meant that large amounts of macroscopic fractures will occur without a large stress increasing. The dynamic fluctuation of AE events also indicated that some relatively large-sized cracks were penetrated and connected. Consequently, this was an AE precursor to the impending destruction of rocks. Therefore, the rock deformation stage was very important for its damage evaluation. Then, according to the evolution characteristics of AE events, the damage state can be distinguished, and the appropriate damage evolution equation can be selected to quantitatively characterize the damage evolution pattern of rocks. Subsequently, the first damage point ($D = 0.375$) was defined and determined based on the turning point of damage variables. Based on the mutation of AE events, the second damage point ($D = 0.5$) was also defined and determined. Absolutely, it was known as the start point of the critical failure stage. Therefore, it is helpful for the prediction of time-to-failure of rocks and the early warning of rockburst.

The damage variable is an indicator for evaluating fracture and damage state of rocks. It can reflect the evolution characteristics of cracks inside rock materials. Through theoretical analysis, it can be learned that the damage evolution curve of rock specimens followed the exponential function law, as shown in Figure 5. By fitting the damage variables with an exponential function, the critical accelerated failure phenomenon can be clearly characterized, and the quantitative evaluation of rock damage can be realized. This provides the basis for realizing the mathematical characterization of rock damage and predicting time-to-failure of rocks. Therefore, based on the damage evolution curve, the first damage point ($D = 0.375$) was defined and determined. Before this point, the damage evolution rate was slow and gradual. After this point, the damage evolution rate grew rapidly. Thus, the first damage point can be used to distinguish differences of damage evolution growth for rocks. Then, according to the actual fracture situations of rocks, the second damage point ($D = 0.5$) was also defined and determined. Correspondingly, the second damage point ($D = 0.5$) can be used to distinguish the stable deformation stage and the critical acceleration failure stage. It can be confirmed by the evolution pattern of AE signals, especially the AE precursor of rock failure occurred after this point, which verified the rationality of the defined second damage point. Accordingly, by defining different damage turning points, the predicting accuracy of rock failure time can be improved.

Based on the first damage point, the damage evolution state of rocks was distinguished, and by the second damage point, the fracture evolution state of rocks was distinguished. No matter from the first damage point to rock failure or from the second damage point to rock failure, the damage state of rocks was in an accelerated growth stage. Moreover, from these two damage points to rock failure, the damage variables roughly showed a linear rapid growth trend. Therefore, it seems possible to predict the failure time of rocks by linear fitting equations. Consequently, based on the damage evolution characteristics, from the second damage point to rock failure, the time-to-failure of rocks was calculated by linear fitting equations, as shown in Figure 7. Moreover, it can be seen that the fitting results were fitted better. This demonstrated that it was reasonable and reliable to fit rock damage evolution pattern by linear equation. Obviously, the results of the fitting equation, from the second damage point to rock failure, had a better linear fitting effect, and the predicted time-to-failure of rocks was more accurate. The damage state and fracture state can be distinguished by the first damage point and the second damage point, which narrowed the data range of the linear fitting of rock damage. However, the deformation of rocks was unstable in the critical failure stage, and the evolution trend of damage variables was unstable. This reduced the prediction accuracy of time-to-failure of rocks due to the local dispersion of damage variables. Therefore, for improving the prediction accuracy, it is necessary to average the damage variables to reduce the predicting errors for time-to-failure of rocks which is caused by the discrete damage variables.

Due to the discontinuity of rock fracture, the average treatment of damage variables can reduce the prediction errors caused by data concentration and unevenness to some extent. It can improve the prediction accuracy by homogenizing and smoothing the discrete data. From the fitting results of Line 1 and Line 2 in Figure 7, it can be seen that the fitting effect of Line 2, with the average of five damage variables, is better than that of Line 1, with the average of two damage variables. It should be noted that this method

has a better fitting effect on processing data with larger discreteness than the data with a more concentrated distribution. For improving the predicting accuracy, a phased calculation method can be used for the early warning of rockburst. The results showed that the predicting time-to-failure of rocks by exponential function will make the results unstable and inaccurate due to the discreteness of damage variables. However, the linear evolution pattern of rock damage can be achieved by averaging damage variables, which had a good effect on improving the prediction accuracy. In fact, it will contribute to the early warning of rock dynamic disasters.

6. Conclusions

Based on the AE signals monitoring experiment and the uniaxial compression test, the time-to-failure of red sandstone was studied and analyzed, and the following conclusions can be obtained.

(1) The red sandstone had stable deformation stage and accelerated failure stage under uniaxial compression. In the stable deformation stage, the stress grew relatively smoothly and AE events were relatively quiet with lower values. In the acceleration failure stage, the stress increased slightly and AE events showed a jump-increase phenomenon with large fluctuation. From the positioning results of AE events, it can be known that the crack penetration mainly occurred in the critical failure stage.

(2) Rock damage obeyed the growth pattern of exponential function under axial loading, and rock damage variables had the steady increase stage and the accelerated increase stage. Moreover, different damage acceleration turning points will affect the linear characterization of acceleration damage stage, and it can further affect the predicting accuracy of rock failure time.

(3) Based on different damage acceleration turning points, the linear fitting effect will be quite different. The linear fitting effect from $D = 0.5$ to rock failure will be better than $D = 0.375$ to rock failure. The averaging processing method of damage variables (from $D = 0.5$ to rock failure) can improve the linear fitting effect and the accuracy of predicting time-to-failure of rocks.

Data Availability

The data used to support the findings of this study are included within the article.

Conflicts of Interest

The authors declare that they have no conflicts of interest.

Acknowledgments

This study was supported by the National Natural Science Foundation of China (Grant Nos. 12172036 and 51774018).

References

[1] X. Lei, K. Kusunose, M. V. M. S. Rao, O. Nishizawa, and T. Satoh, "Quasi-static fault growth and cracking in homogeneous brittle rock under triaxial compression using acoustic emission monitoring," *Journal of Geophysical Research: Solid Earth*, vol. 105, no. B3, pp. 6127–6139, 2000.

[2] A. F. Bell, J. Greenhough, M. J. Heap, and I. G. Main, "Challenges for forecasting based on accelerating rates of earthquakes at volcanoes and laboratory analogues," *Geophysical Journal International*, vol. 185, no. 2, pp. 718–723, 2011.

[3] A. F. Bell, M. Naylor, and I. G. Main, "The limits of predictability of volcanic eruptions from accelerating rates of earthquakes," *Geophysical Journal International*, vol. 194, no. 3, pp. 1541–1553, 2013.

[4] A. F. Bell, "Predictability of landslide timing from quasi-periodic precursory earthquakes," *Geophysical Research Letters*, vol. 45, no. 4, pp. 1860–1869, 2018.

[5] J. Vasseur, F. B. Wadsworth, Y. Lavallée, A. F. Bell, I. G. Main, and D. B. Dingwell, "Heterogeneity: the key to failure forecasting," *Scientific Reports*, vol. 5, no. 1, article 13259, 2015.

[6] X. L. Li, S. J. Chen, Q. M. Zhang, X. Gao, and F. Feng, "Research on theory, simulation and measurement of stress behavior under regenerated roof condition," *Geomechanics and Engineering*, vol. 26, no. 1, pp. 49–61, 2021.

[7] X. L. Li, S. J. Chen, S. M. Liu, and Z. H. Li, "AE waveform characteristics of rock mass under uniaxial loading based on Hilbert-Huang transform," *Journal of Central South University*, vol. 28, no. 6, pp. 1843–1856, 2021.

[8] B. Voight, "A method for prediction of volcanic eruptions," *Nature*, vol. 332, no. 6160, pp. 125–130, 1988.

[9] M. J. Heap, P. Baud, P. G. Meredith, A. F. Bell, and I. G. Main, "Time-dependent brittle creep in Darley Dale sandstone," *Journal of Geophysical Research*, vol. 114, no. B7, article B07203, 2009.

[10] T. Fukuzuno, "A method to predict the time of slope failure caused by rainfall using the inverse number of velocity of surface displacement," *Landslides*, vol. 22, no. 2, pp. 8–13_1, 1985.

[11] A. Boué, P. Lesage, G. Cortés, B. Valette, and G. Reyes-Dávila, "Real-time eruption forecasting using the material failure forecast method with a Bayesian approach," *Journal of Geophysical Research: Solid Earth*, vol. 120, no. 4, pp. 2143–2161, 2015.

[12] N. Brantut, M. J. Heap, P. G. Meredith, and P. Baud, "Time-dependent cracking and brittle creep in crustal rocks: a review," *Journal of Structural Geology*, vol. 52, pp. 17–43, 2013.

[13] Z. T. Bieniawski, "Time-dependent behaviour of fractured rock," *Rock Mechanics*, vol. 2, no. 3, pp. 123–137, 1970.

[14] S. F. M. Chastin and I. G. Main, "Statistical analysis of daily seismic event rate as a precursor to volcanic eruptions," *Geophysical Research Letters*, vol. 30, no. 13, article 1671, 2003.

[15] R. R. Cornelius and P. A. Scott, "A materials failure relation of accelerating creep as empirical description of damage accumulation," *Rock Mechanics and Rock Engineering*, vol. 26, no. 3, pp. 233–252, 1993.

[16] W. Weibull, "A statistical distribution function of wide applicability," *Journal of Applied Mechanics*, vol. 18, no. 3, pp. 293–297.

[17] Z. L. Wang, Y. C. Li, and J. G. Wang, "A damage-softening statistical constitutive model considering rock residual strength," *Computers & Geosciences*, vol. 33, no. 1, pp. 1–9, 2007.

[18] J. B. Keats, F. R. Lawrence, and F. K. Wang, "Weibull maximum likelihood parameter estimates with censored data," *Journal of Quality Technology*, vol. 29, no. 1, pp. 105–110, 2018.

[19] E. Hoek and E. Brown, *Underground Excavation in Rock, Institution of Mining and Metallurgy*, CRC Press, Taylor & Francis Group, London, 1980.

[20] G. D. Hutcheson, *Ordinary Least-Squares Regression*, The Multivariate Social Scientist, SAGE Publications Ltd, London, 1999.